JOURNAL OF THERMOPHYSICS AND HEAT TRANSFER
Vol. 8, No. 2, April–June 1994

# Macroscopic Spread Function Analysis for Subsurface Scattering of Semitransparent Materials

B. K. Tsai* and D. P. DeWitt†
*Purdue University, West Lafayette, Indiana 47907*
and
G. H. Shaffer‡
*Miles Laboratories, Inc., Elkhart, Indiana 46515*

**The macroscopic spread function describes the extent to which radiation is spread in a semitransparent material due to surface and subsurface scattering. The objective of this article is to investigate the effects of optical and geometrical parameters on the macroscopic spread function of plastic reference samples. Experimental measurements showed that least spreading was associated with the off-white plastic samples using a wavelength of 700 nm and a reflected angle of 55 deg. A flexible Monte Carlo (MC) model developed to predict the spatial distribution of reflected energy incorporated the complete scattering distribution as well as the scattering and absorption processes. The simulation results revealed that least spreading occurred for the off-white samples at 700 nm and with a 45-deg reflected angle. When the experimental and MC results were compared, it was found that most spreading was associated with the forward scattering distribution, while least spreading developed when using the backward distribution. In addition, the experimental data best matched the simulations using the backward scattering distribution.**

## Nomenclature

$B$ = isotropic scattering in the backward direction with no forward scattering
$D$ = sample width, mm
$d$ = illumination diameter, mm
$F$ = isotropic scattering in the forward direction with no backward scattering
$I$ = directional incident intensity, W/m$^2$/$\mu$m
$L$ = path length traveled by photon
$n$ = refractive index relative to that of air
$P$ = scattering phase function
$R$ = random number
$S$ = spreading factor
$\mathcal{S}$ = spread function
$t$ = sample thickness, mm
$U$ = uniform or isotropic scattering distribution
$x$ = distance along the surface
$\Delta x$ = scale of output grid
$\theta$ = angle from normal
$\kappa$ = absorption coefficient, mm$^{-1}$
$\lambda$ = wavelength
$\xi$ = dummy variable for $x^*$ axis
$\pi$ = 3.14159
$\sigma$ = scattering coefficient, mm$^{-1}$

*Subscripts*
$e$ = exitent
$i$ = incident
$L$ = pertaining to path length
$m$ = Monte Carlo
$r$ = refracted; reflectometric
$\kappa$ = pertaining to the absorption coefficient

*Superscripts*
$*$ = normalized; dummy variable

Received May 3, 1993; presented as Paper 93-2803 at the AIAA 28th Thermophysics Conference, Orlando, FL, July 6–9, 1993; revision received Aug. 13, 1993; accepted for publication Aug. 25, 1993.

*Research Assistant, Mechanical Engineering Department. Student Member AIAA.
†Professor, Mechanical Engineering Department. Member AIAA.
‡Senior Staff Engineer, Diagnostics Division.

## Introduction

SCATTERING is a redirection of energy in which not all of the incoming energy is lost.[1] A comprehension of the effects of optical and geometrical parameters on subsurface scattering, along with a sufficient knowledge of the underlying mechanisms that influence subsurface scattering, is required for developing correct models to predict scattering behavior and for making accurate engineering decisions concerning scattering problems. Applications for which subsurface scattering plays an important role are myriad and range from the atmospheric sciences[2,3] to biological studies.[4] The particular area of interest here deals with subsurface scattering in semitransparent materials for reflectometric applications, but the principles and tools presented in this article are applicable to other situations as well.

Most of the semitransparent scattering studies to date have been done in one dimension and deal with apparent properties of the whole media.[5,6] Recently, some studies dealing with two and three dimensions have emerged. Early experimental works by some Russian authors were the first to publish any type of spreading data,[7–11] but these studies dealt only with paper products. Two-dimensional Monte Carlo (MC) simulations that have been performed include the works of Jentink et al.[12] and Tränkle and Greenler.[13] Analytical techniques for the solution of the radiative transfer equation have been used to model the spatial distribution of reflected intensities from a material. Among these are the studies of Crosbie and Koewing[14] and Kim and Lee.[15] Thus, much of the literature on spread functions has been focused on thin layers and has assumed isotropic scattering in transparent media, such as biological fluids, and has not treated anisotropic scattering in semitransparent materials, such as plastics.

## Background

Consider a uniform, collimated beam incident on a semitransparent sample as shown in Fig. 1. The vertical dashed

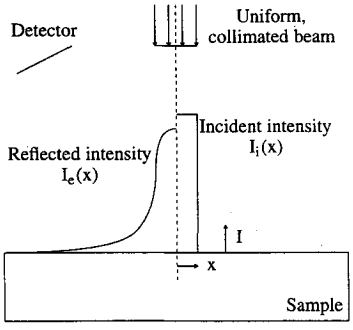


**Fig. 1 Physics of the macroscopic spread function.**

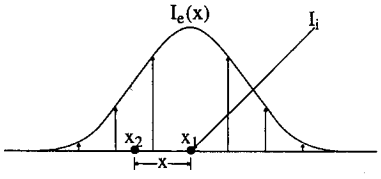


**Fig. 2 The macroscopic spread function.**

line represents the centerline from which the radial distance $r$ is measured. The two labeled directional intensity distributions $I_e$ and $I_i$ describe the front surface and are positive upwards as shown. When this sample is irradiated by an incident intensity distribution $I_i(x)$, radiation is scattered in two ways. First, radiation will be reflected from the surface irregularities according to Fresnel reflection. Second, the incident radiation which penetrates the surface will be scattered from different depths beneath the surface, some of which will leave the surface from which it entered. The macroscopic spread function is then the spatial distribution of the intensity $I_e(x)$ that exits the surface due to surface and subsurface scattering. This function, which from now on will be called the spread function, can be defined as the ratio of the intensity of exitent radiation at a surface point $x_e$ to the irradiance at an incident surface point $x_i$ (see Fig. 2). In symbolic form, the function can be written as

$$\mathcal{S}(x_e; x_i) = I_e(x_e)/I_i(x_i) \tag{1}$$

The assumption of a homogeneous medium allows the spread function to be expressed as

$$\mathcal{S}(x) = I_e(x)/I_i \tag{2}$$

Knowledge of the spread function is important to the design of reflectometers, where the ratio of reflected radiance for a sample to that for a reference is measured. The percentage of energy collected using a particular field of view can be calculated from a spread function. The error in reflectometric measurements can result from the field of view being narrower than the spread function. Incorrect reflection values can result if the reflectometer is sensitive to target size or to the spread function of the sample. Broad spread functions may result in low systematic reflection values, while differences in the spread function from sample to sample will result in random errors in the reflection values.

## Experimental Study

Two types of 0.381-mm-thick molded acrylonitrile butadiene styrene (ABS) plastic samples[16] (74% reflectance off-white, 92% reflectance white) were measured with an illumination diameter of 0.4 mm at two wavelengths (700 and 800 nm) and three exitent angles (45, 55, and 65 deg as measured from the normal).

### Setup and Procedure

The spread function was measured by the fast raster area scattering instrument (FRASI) (Fig. 3). The plastic samples

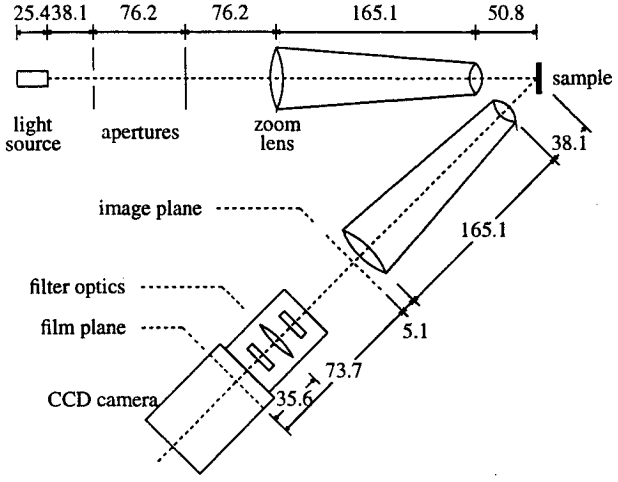


**Fig. 3 FRASI setup for measuring the MSF (dimensions in millimeters).**

were irradiated with broadband light, passed through an auxiliary aperture, a primary aperture, and transfer optics. After reflecting off the samples, the light was passed through Corion® interference filters (700 ± 12.5 nm, 800 ± 12.5 nm) before reaching the charge-coupled device (CCD) detector array (512 by 480 pixels in a 60 × 80-mm area). A data acquisition program, embodied in the FRASI software, captured and stored the data.

Samples were placed in a consistent orientation onto a vertical platform, and care was exercised to place samples such that the illumination beam was centered on the sample (except for uniformity measurements as will be explained later). Before each combination of incident beam diameter and filter color, the reference signal was obtained by measuring a Spectralon™ sample using a large 5-mm-diam incident beam. The images in two orthogonal directions (512 data points in the vertical direction and 480 data points in the horizontal direction) were recorded by the detector and transmitted through a camera controller to the microcomputer for numerical calculations. The images were also displayed on a black and white monitor. Observations for both the reference and the sample readings were captured by the data acquisition system only after careful steps were made to assure adequate and proper detector power levels.[16]

Five repeatability measurements separated by 1-min intervals were made on the same sample with the same experimental conditions (geometrical and optical properties). Five uniformity measurements were made with the incident beam placed at different locations on the sample surface. Ten samples were involved in each sample-to-sample variability study.

### Results

All data sets have been smoothed with a low-pass digital filtering technique, called the Parks-McClellan algorithm. The abscissa for all of the spreading graphs are normalized by

$$x^* = (\cos \theta_i/d)(2x - D) \tag{3}$$

A spreading factor defined by

$$S = 1 - \left[\int_{-1}^{1} \mathcal{S}(\xi)\, d\xi \Big/ \int_{-\infty}^{\infty} \mathcal{S}(\xi)\, d\xi\right] \tag{4}$$

describes how much of the incoming energy has been lost to the region outside the illumination diameter.

The variability parameters [as indicated by the standard-deviation-to-mean (SDTM), ratio at $x^* = 0$] for instrument repeatability, sample uniformity, and sample variability are about ±8.3%, ±8.7%, and ±34.4%, respectively. Param-

eters for instrument reproducibility and sample uniformity of the off-white plastic sample indicate lower spreading factor SDTM ratios than the sample variability parameter.

Although the influence of wavelength on FRASI measurements is expected to be small due to the little difference between the scattering and absorption coefficients at 700 and 800 nm, the slight difference does affect the amount of spreading. In the results of Fig. 4 for the off-white sample, the bidirectional scattering distribution function (BSDF) spreads slightly more at the longer wavelength. The scattering-to-absorption ratio is slightly higher at 800 nm, and thus is consistent with the data. The reverse effect of a lower scattering-to-absorption ratio at the longer wavelength for the white sample is shown in Fig. 5. In this plot, it is shown that more spreading occurs at the shorter wavelength. This is in agreement with the higher scattering-to-absorption ratios at the shorter wavelength for the white sample.[16]

Concerning reflected angles, the level of spreading from highest to lowest occurs in this order: $\theta_e$ = 45, 65, and 55 deg (see Fig. 6). There appears to be an optimum angle in the range from 45–65 deg in which minimum spreading can be achieved. The reason for least spreading at the intermediate reflected angle, 55 deg, is due to a combination of effects that produce least spreading at 45-deg reflected angle, and those that produce least spreading at 65-deg reflected angle. For example, least energy would be spread to the wings and then to the detector with the 45-deg reflected angle due to the smaller solid angles, but most energy would be spread to the wings and to the detector with the 45-deg reflected angle due to a reflectance distribution that obeys neither the lambertian distribution nor the Fresnel relationships.

The white plastic material spreads more than the off-white material (see Fig. 7). This is to be expected, since the scattering-to-absorption is an order of magnitude larger in the white samples than in the off-white samples.[16] The results of average spreading factors in Table 1 are consistent with the observations described in the previous three paragraphs. (Total means the average for all of the measurements of one material.)

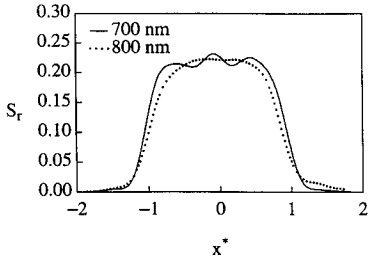


**Fig. 4 Influence of wavelength for off-white samples at 45-deg reflected angle.**

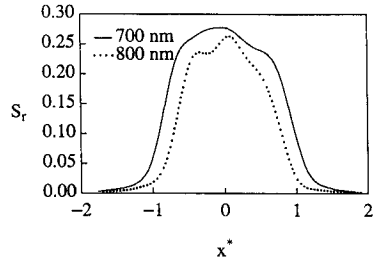


**Fig. 5 Influence of wavelength for white samples at 55-deg reflected angle.**

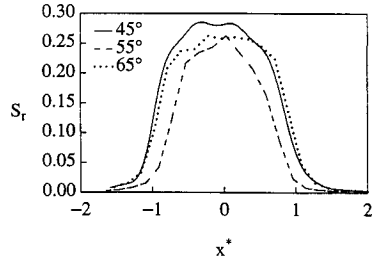


**Fig. 6 Influence of reflected angle for off-white samples measured at 800 nm.**

**Table 1 Average spreading factors, %**

| | Off-white plastic | | |
|---|---|---|---|
| | 700 nm | 800 nm | Total |
| Experimental | 5.1 | 5.2 | 5.1 |
| Monte Carlo | 8.10 | 8.23 | 8.17 |
| | White plastic | | |
| Experimental | 8.7 | 8.0 | 8.3 |
| Monte Carlo | 7.63 | 9.86 | 8.75 |
| | Angle | | |
| | 45 Deg | 55 Deg | 65 Deg |
| Experimental | 8.7 | 4.1 | 7.4 |
| Monte Carlo | 8.43 | 8.42 | 8.53 |

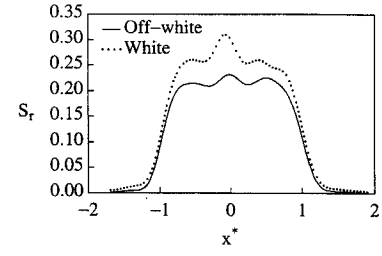


**Fig. 7 Influence of material for 45-deg reflected angle measured at 700 nm.**

## Monte Carlo Modeling

A major thrust of this study was the development of a MC ray tracing program capable of simulating experimental spread function and BSDF data. The influences of subsurface scattering and absorption, as well as front and back surface reflection and transmission phenomena, were incorporated into the MC scheme. A Fortran code was first written and tested on mainframe computers at Purdue University before it was converted into the final QuickBASIC version for utility in industrial situations. Verification of the code was achieved by comparison with the results available in the literature.

### Model

The basic assumptions employed in the MC code are a homogeneous material, Snell's Law of refraction, and an isothermal, cold medium. The flexibility of this MC model allows for inputs of geometrical dimensions, optical parameters, and choice of various options. The outputs from the MC code are the spread function and the following statistics: a breakdown of what happened to the rays, the number of scattering events, number of interactions per trace, and the cpu and real time required to run the program.

Each trace begins by generating a random position on the aperture and directing the ray to the front surface (Fig. 8). The ray is reflected and traced to the detector plane if $R_\rho \leq \rho$. Otherwise, it is transmitted into the sample. It then travels a path length defined by

$$L = -(\ln R_L)/(\kappa + \sigma) \tag{5}$$

Then the ray is absorbed if $R_\kappa \leq \kappa$. If not, it is scattered in a new direction as modified by

$$R_\theta = \left[\int_0^\theta P(\theta^*)\, d\theta^* \Big/ \int_0^{2\pi} P(\theta^*)\, d\theta^*\right] \tag{6}$$

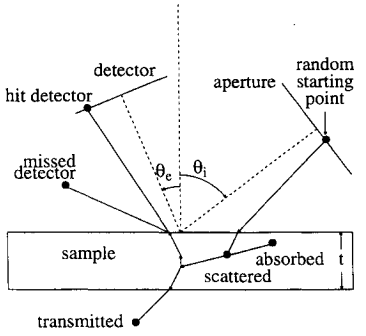


**Fig. 8 Monte Carlo ray tracing setup.**

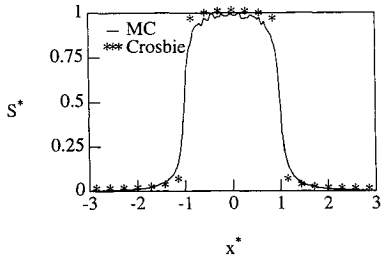


**Fig. 9 Two-dimensional Monte Carlo validation.**

A ray reaching the front or back surface can be reflected back into the sample or transmitted out of the sample. Once a ray reaches a detector, it is counted as a successful ray. If the ray is absorbed, is transmitted through the back surface, or missed the detector, then the ray is counted lost, and the trace is restarted. This process is repeated until the number of successful rays or total rays sent has been reached.

### Validation

The MC model has been validated by comparison with the two-dimensional plane-layer results of Crosbie and Koewing.[14] The comparison indicates that more disparity occurs at high scattering. The results in Fig. 9 for a scattering albedo of unity and an optical thickness of 0.2 show that the MC model is reasonable.

### Results

A suite of 12 simulations implementing uniform scattering distributions was performed to match the experimental conditions. The set consists of two types of plastic materials (off-white and white) using two wavelengths (700 and 800 nm, chosen to match the optical characteristics of the reagent strips used) and three exitent angles (45, 55, and 65 deg). Appropriate scattering and absorption coefficients as predicted from the Kubelka-Munk equations[17] and an assumed scattering phase function composed the input set describing the material. The wavelength was incorporated into the model by using spectral absorption and scattering coefficients that are functions of wavelength. The exitent angle, of course, along with the incident angle, was a direct input into the program.

Simulation variability was assessed by running the same simulation 10 times and calculating the centerline SDTM ratio and the spreading factor SDTM ratio. The result was a SDTM ratio of about $\pm 1.0\%$. Although this is about twice that of the sample-to-sample variability ($\pm 0.34\%$) reported in the experimental results, it is a tolerably small ratio when compared with the sample-to-sample variability of the plastic sample ($\pm 3.2\%$). The centerline SDTM ratio represents the errors associated with the computing process itself, such as roundoff error, transcendental function approximation, $n$-bit accuracy, error propagation, and random number generation. The spreading factor SDTM ratio, $\pm 0.6\%$, indicates the precision to which the spreading factor may be predicted.

The influence of wavelength was first investigated. As expected, the effect of wavelength was almost insignificant. From the graphs, it was difficult to ascertain the wavelength at which more spreading was present. For example, in Fig. 10, it appears that the graph for 700 nm loses slightly more energy through the wings of the plot, but, in fact, it loses slightly less energy through the sides.

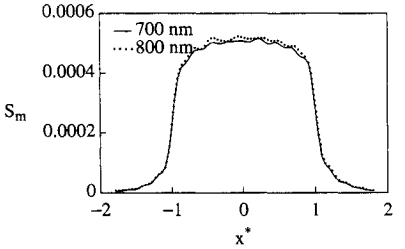


**Fig. 10 Influence of wavelength for off-white samples predicted at 45-deg reflected angle.**

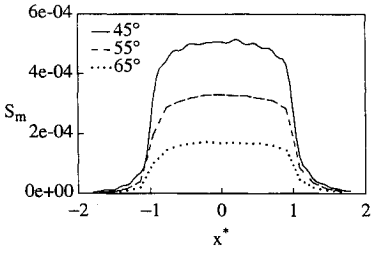


**Fig. 11 Influence of reflected angle for off-white samples predicted at 700 nm.**

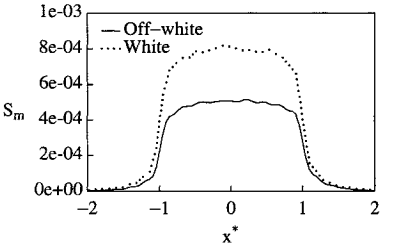


**Fig. 12 Influence of material for 45-deg reflected angle predicted at 700 nm.**

The effect of reflected angle is shown in Fig. 11 for simulation of off-white plastic samples measured at 700 nm. The results predict more energy collected at the lower reflected angle. It is difficult to distinguish the spreading factors among the different reflected angles.

Plastic material effects were as expected. The white plastic reflects more energy and spreads slightly more than the off-white sample. This is in agreement with the fact that the white material has a higher scattering-to-absorption ratio than the off-white material (see Fig. 12).

It is evident from the MC results in Table 1 that more spreading occurs at $\lambda = 800$ nm for both materials. A reason for the absence of the material effect as observed in the experimental results is the insufficient knowledge of the scattering distribution. It could be suggested from Table 1 that the highest reflected angle ($\theta_e = 65$ deg) provides the most spreading, but the spreading factors are too close to determine which of the two reflected angles provides the least spreading. The disparity between this result and the experimental results can be attributed to incorrect MC assumptions, such as uniform, collimated incident radiation and a Fresnel reflectance distribution. The spreading factors indicate slightly higher spreading for the white samples. In general, these results confirm those of the experimental data.

## Comparison

For the purpose of comparison, the results for both the experimental and the numerical studies were normalized such

that the maximum value was unity. The results are given in Figs. 13–16.

For $\theta_e$ = 45 deg and $\theta_e$ = 65 deg, the MC results exhibit greater spreading than the experimental data for the off-white sample, but the reverse result is true for the white sample. This behavior is evident for the off-white sample in Fig. 13, where the MC results show more spreading than the experimental results, and for the white sample in Fig. 14 where the opposite is apparent. For $\theta_e$ = 55 deg, the MC results display less spreading than the experimental results (see Fig. 15).

As can be seen from Fig. 16, among the three basic scattering distributions, the forward scattering distribution produced the highest spreading, and the backward scattering distribution produced the least spreading. Most spreading would be expected from the forward scattering distribution because the tendency for the photon to continue in a forward direction away from the light source causes in general a beam broadening effect. On the other hand, beam broadening is suppressed when using the backward scattering distribution because the photons tend to deflect back towards the front surface upon reaching the first scattering center. A uniform distribution maintains a balance of these effects. This trend is clearly seen in Table 2. (Total means the average for all of the measurements for the particular scattering distribution.)

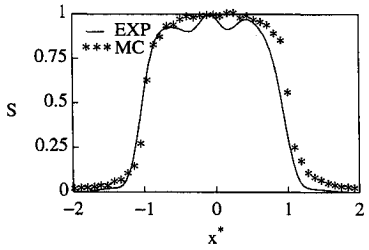


**Fig. 13 Comparison of MC and EXP results for an off-white plastic sample measured with 45-deg incident angle and at 700 nm.**

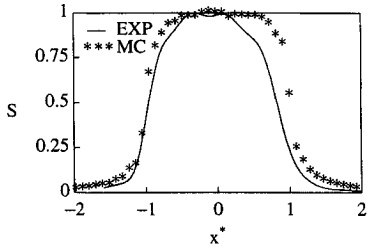


**Fig. 14 Comparison of MC and EXP results for a white plastic sample measured with 45-deg incident angle and at 800 nm.**

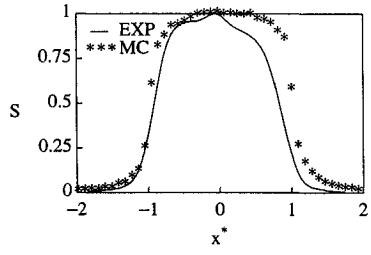


**Fig. 15 Comparison of MC and EXP results for an off-white plastic sample measured with 55-deg incident angle and at 700 nm.**

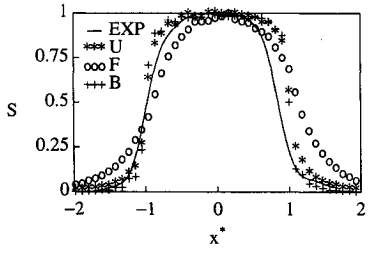


**Fig. 16 Comparison of Monte Carlo and experimental results for an off-white plastic sample measured with 45-deg incident angle and at 800 nm.**

**Table 2 Comparison of average spreading factors for different scattering distributions**

| Variable | Experimental | *U* | *F* | *B* |
|---|---|---|---|---|
| 700 nm, off-white | 5.1 | 8.1 | 20.8 | 5.2 |
| 700 nm, white | 5.2 | 7.6 | 21.2 | 5.3 |
| 800 nm, off-white | 8.7 | 8.2 | 17.7 | 5.0 |
| 800 nm, white | 8.0 | 9.9 | 22.1 | 6.5 |
| 45 Deg | 9.6 | 8.43 | 20.43 | 5.48 |
| 55 Deg | 5.5 | 8.42 | 20.46 | 5.52 |
| 65 Deg | 7.5 | 8.53 | 20.38 | 5.53 |
| Off-white | 5.7 | 8.2 | 21.0 | 5.3 |
| White | 8.3 | 8.7 | 19.9 | 5.8 |
| Total | 6.7 | 8.5 | 20.4 | 5.5 |

For $\theta_e$ = 55 deg, the MC results demonstrate less spreading than the experimental results, while the converse is true for the other two reflected angles. Overall, the order of spreading from highest to lowest as measured by the spreading factor is as follows: forward, uniform, experimental, backward. The results suggest that the experimental scattering distribution can be best approximated by a uniform or backward scattering distribution, and that the forward scattering distribution can be excluded from the set of possible scattering distribution approximations. The backward scattering distribution is appropriate for estimating the area outside the illumination spot, but still can be improved to approximate the main body of the BSDF.

## Conclusions and Recommendations

The spread function is key to describing the reflective properties of semitransparent materials. New contributions in this study are the use of BSDF data as a measure of the spreading in a semitransparent material and the flexible MC model, which can be utilized to simulate the spreading behavior in a material. At present, spread function data is sparse, especially for bulk materials such as plastics.

Filter wavelengths, reflected angles, and plastic material affect the spread function. Least spreading occurred with the off-white sample using the 700-nm filter. Experimental results indicate least spreading with 55-deg reflected angle, while the MC results reveal least spreading with 45-deg angle. The difference is due to incorrect assumptions employed in the MC model.

Two issues of interest for future research are recommended. First, an optimization study can be conducted to determine if indeed reflected angles exist for which spreading is minimized and what those angles are. Second, a study of surface characteristics (such as roughness, power spectral density, etc.) can be performed to discover their influence on the spread function.

## Acknowledgments

Funding for this project was made possible by Miles, Inc., Elkhart, Indiana. The authors gratefully acknowledge the collaboration of John Stover from TMA Technologies, Inc. in Bozeman, Montana. Thanks are given to R. O. Buckius (University of Illinois at Urbana-Champaign) for helpful advice with the MC modeling, A. Crosbie (University of Missouri at Rolla) for insightful conversations on model validation, and P. Davies (Purdue University, West Lafayette, Indiana) for guidance with digital filtering techniques.

## References

[1]Siegel, R., and Howell, J. R., "Thermal Radiation Heat Transfer," Hemisphere, New York, 1981.

[2]Farrukh, U. O., "Multiple Scattering for Laser Beams Propagating in a Layered Atmosphere," *Laser Radar Technology and Applications*, Vol. 663, Quebec City, Canada, June 1986, pp. 57–64.

[3]Kumer, J. B., "Polarization of Multiple Scattered Light in Planetary Atmospheres from Solution of the Coupled Linear Integral Equations Derived for Mixed Rayleigh-Isotropic Scattering," *Journal of Quantitative Spectroscopy and Radiative Transfer*, Vol. 14, Feb. 1973, pp. 165–187.

[4]Fukshansky, L., Fukshansky-Kazarinova, N., and Von Remisowsky, A. M., "Estimation of Optical Parameters in a Living Tissue by Solving the Inverse Problem of the Multiflux Radiative Transfer," *Applied Optics*, Vol. 30, No. 22, 1991, pp. 3145–3153.

[5]Hogg, C. S., "The Application of Kubelka-Munk Theory to the Study of Translucent Ceramic Systems," *Proceedings of the British Ceramic Society*, Vol. 28, June 1979, pp. 23–35.

[6]Thomas, M. B., and Doremus, R. H., "Characterizing Opacity of Translucent Ceramic Materials," *Journal of the American Ceramic Society*, Vol. 59, No. 5, 1976, pp. 229–232.

[7]Voishvillo, N. A., "Dependence on the Properties of Radiation Leaving the Plane Layer of a Scattering Medium on Its Thickness," *Optics and Spectroscopy (USA)*, Vol. 42, No. 5, 1977, pp. 545–548.

[8]Voishvillo, N. A., Blinova, L. D., and Khapugina, E. I., "Experimental Study of the Angular Distribution of Radiation Passing Through Flat Layers of a Scattering Medium," *Journal of Applied Spectroscopy*, Vol. 43, No. 6, 1977, pp. 678–683.

[9]Voishvillo, N. A., "Study of the Spreading of a Finite Beam Transmitted Through a Scattering Layer," *Journal of Applied Spectroscopy*, Vol. 42, No. 6, 1985, pp. 694–698.

[10]Il'yasov, S. G., Krasnikov, V. V., Tyurev, E. P., and Ageenko, I. S., "Improved Two-Beam Specular Hemisphere Method for Measuring Thermal Radiation Characteristics of Scattering Materials," *Journal of Engineering Physics (USA)*, Vol. 32, No. 5, 1977, pp. 487–491.

[11]Il'yasov, S. G., Krasnikov, V. V., and Tyurev, E. P., "Methods of Examining Beam Diffusion in an Absorbing and Scattering Material," *Journal of Engineering Physics (USA)*, Vol. 32, No. 2, 1977, pp. 161–164.

[12]Jentink, H. W., De Mul, F. F. M., Hermsen, R. G. A. M., Graaf, R., and Greve, J., "Monte Carlo Simulations of Laser Doppler Blood Flow Measurements in Tissue," *Applied Optics*, Vol. 29, No. 16, 1988, pp. 2371–2381.

[13]Tränkle, E., and Greenler, R. G., "Multiple-Scattering Effects in Halo Phenomena," *Journal of the Optical Society of America A*, Vol. 4, No. 3, 1987, pp. 591–599.

[14]Crosbie, A. L., and Linsenbardt, T. L., "Two-Dimensional Isotropic Scattering in a Semi-Infinite Medium," *Journal of Quantitative Spectroscopy and Radiative Transfer*, Vol. 19, No. 3, 1978, pp. 257–284.

[15]Kim, T. K., and Lee, H. S., "Radiative Transfer in Two-Dimensional Anisotropic Media with Collimated Incidence," *Journal of Quantitative Spectroscopy and Radiative Transfer*, Vol. 42, No. 3, 1989, pp. 225–238.

[16]Tsai, B. K., "Macroscopic Spread Function Analysis for Subsurface Scattering in Semitransparent Materials," Ph.D. Dissertation, Purdue Univ., West Lafayette, IN, 1993.

[17]Kortüm, G., "Reflectance Spectroscopy: Principles, Methods, Applications," Springer-Verlag, Berlin/Heidelberg, 1968.